

Growing 1D and Quasi-2D Unstable Manifolds of Maps

Bernd Krauskopf^{*,1} and Hinke Osinga^{†,2}

**Theoretical Physics, Vrije Universiteit, De Boelelaan 1081, 1081 HV Amsterdam, The Netherlands; and*

†The Geometry Center, University of Minnesota, 400 Lind Hall, Minneapolis, Minnesota 55455

E-mail: *berndk@nat.vu.nl and †hinke@geom.umn.edu

Received February 16, 1998; revised June 30, 1998

We present a new 1D algorithm for computing the global one-dimensional unstable manifold of a saddle point of a map. Our method can be generalized to compute two-dimensional unstable manifolds of maps with three-dimensional state spaces. This is shown here with a quasi-2D (Q2D) algorithm for the special case of a quasiperiodically forced map, which allows for a substantial simplification of the general case described in Krauskopf and Osinga (1998). The key idea is to “grow” the manifold in steps, which consist of finding a new point on the manifold at a prescribed distance from the last point. The speed of growth is determined only by the curvature of the manifold, and not by the dynamics.

The performance of the 1D algorithm is demonstrated with a constructed test example, and it is then used to compute one-dimensional manifolds of a map modeling mixing in a stirring tank. With the Q2D algorithm we compute two-dimensional unstable manifolds in the quasiperiodically forced Hénon map. © 1998 Academic Press

1. INTRODUCTION

Many interesting dynamical systems are given by a map from a state space to itself, describing the evolution of a state of the system by iteration. The map may either be explicitly defined, as for example the Hénon map [12] and the Ikeda map [11, 16], or appear in the form of the Poincaré map of a vector field, as in the forced Van der Pol and Duffing oscillators [10]. Of great importance for understanding the dynamics is the knowledge of the stable and unstable manifolds of invariant objects of saddle type, such as

¹ Current address: Department of Engineering Mathematics, University of Bristol, Bristol BS8 1TR, UK. E-mail: b.krauskopf@bristol.ac.uk.

² Current address: Control and Dynamical Systems, California Institute of Technology, Mail Stop 107-81, 1200 East California Boulevard, Pasadena, California 91125. E-mail: hinke@cds.caltech.edu.

saddle points and invariant circles and tori. These manifolds organize the global dynamics of the system and they can have extremely complicated embeddings into the phase space. A transverse intersection of stable and unstable manifolds leads to horseshoe dynamics [25] and is responsible for transport between different regions of phase space [31]. Furthermore, stable manifolds form boundaries between different attractors, and their bifurcations can lead to sudden changes of the attractor [9, 11].

Stable and unstable manifolds are global objects that usually cannot be found analytically, but need to be computed numerically. In many applications one wants to compute increasingly larger pieces of (un)stable manifolds, starting from the saddle point (or circle, or torus), up to a prescribed arclength. Almost all algorithms for the computation of one-dimensional manifolds use iteration of a fundamental domain; see Section 2. This cannot be used for two-dimensional manifolds, because any initial mesh of a fundamental domain for a two-dimensional manifold will quickly degenerate under just a few iterations; see [20].

In this paper we present a 1D algorithm for computing the one-dimensional unstable manifold of a fixed point that can be generalized to compute two-dimensional manifolds. The main idea is to grow the manifold independently of the dynamics in steps as a list of points. At each step a new point is added at a prescribed distance Δ_k from the last point. In order to achieve a good approximation, the distance Δ_k must change from step to step with the curvature of the manifold. We monitor the quality of the approximation with the strategy of Hobson [13]. The performance of this method is demonstrated with two examples: the shear map, a constructed test example, and a blinking vortex map modeling chaotic fluid dynamics in a stirred tank; compare [1, 17, 30]. Examples of computed (un)stable manifolds of Poincaré maps can be found in [18, 19].

We then present a method for the special case of the two-dimensional unstable manifold of a quasiperiodically forced map, which we call the quasi-2D (Q2D) algorithm. This algorithm is a true generalization of the 1D algorithm, and it is substantially simpler than that for the general case of a two-dimensional unstable manifold in [20]. Note that the only other (and very different) method for two-dimensional manifolds of maps is the method of outer approximation in [5, 6, 23]. As an example, we compute the unstable manifold of an invariant circle of the quasiperiodically forced Hénon map. This map is studied in [29] as an example of a map with a strange nonchaotic attractor.

The paper is organized as follows. In Section 2 we introduce some notation and give a brief overview of other methods for computing one-dimensional manifolds. In Section 3 we explain the 1D algorithm and demonstrate its performance with two examples. Section 4 explains how our method can be generalized to obtain the Q2D algorithm. All pictures of manifolds are visualized with Mathematica [32], except Fig. 7, which was rendered with Geomview [27].

2. BACKGROUND

We first discuss the computation of one-dimensional manifolds. To keep the exposition simple, we stay in the context of planar diffeomorphisms; that is, we assume that the map is differentiable and has a differentiable inverse. In this setting the only invariant set of saddle type with (nontrivial) stable and unstable manifolds is a saddle point. Suppose we are given an orientation preserving diffeomorphism $f: \mathbb{R}^2 \rightarrow \mathbb{R}^2$. (This is not a restriction: if f is orientation reversing, consider its second iterate.) Let x_0 be a saddle point of f . Hence,

$f(x_0) = x_0$ and the Jacobian $Df(x_0)$ has two real eigenvalues λ^s and λ^u with $0 < \lambda^s < 1 < \lambda^u$. The unstable manifold of x_0 is defined as

$$W^u(x_0) := \{x \in \mathbb{R}^2 \mid f^{-n}(x) \rightarrow x_0 \text{ as } n \rightarrow \infty\},$$

where f^n denotes the n th iterate of f . Note that, since f is a diffeomorphism, the stable manifold $W^s(x_0)$ of f is the unstable manifold of the inverse f^{-1} . The Unstable Manifold Theorem [24] guarantees the existence of the *local unstable manifold*

$$W_{\text{loc}}^u(x_0) := \{x \in W^u(x_0) \mid f^{-n}(x) \in U \text{ for all } n \in \mathbb{N}\},$$

in a suitable neighborhood U of x_0 . Furthermore, it states that $W_{\text{loc}}^u(x_0)$ is tangent to the unstable eigenspace $E^u(x_0)$ of λ^u .

The idea behind most algorithms is to globalize the local unstable manifold $W_{\text{loc}}^u(x_0)$ by *iterating a fundamental domain*. Pick a point $p \in W_{\text{loc}}^u(x_0)$, such that $f(p) \in W_{\text{loc}}^u(x_0)$. Then the piece of $W_{\text{loc}}^u(x_0)$ between p and $f(p)$ is a fundamental domain F_p , meaning that all orbits on the branch of $W^u(x_0)$ containing p have exactly one point in F_p . In particular, the iterates of F_p will cover this branch of $W^u(x_0)$. To use this idea one needs to compute an approximation of $W_{\text{loc}}^u(x_0)$ in a neighborhood of x_0 . Often the linear approximation $E^u(x_0)$ suffices [33]; see [14, 15, 22, 28] for higher-order approximations of $W_{\text{loc}}^u(x_0)$. Note that it is not possible to iterate F_p as a continuous object, but only as a finite set of points. This results in a set of points approximating $W^u(x_0)$. Extra points must be added in the computation to ensure a good quality of the approximation. There are two strategies: In [28, 33] iterates are taken from points in the original fundamental domain F_p . The alternative is to approximate points in the current iterate of the fundamental domain and apply the map once; this is done in [13, 26].

Our method goes even beyond that by abandoning the idea of iterating a fundamental domain. The idea is to produce a list of points on $W^u(x_0)$ by successively adding new points at prescribed distances from the last point. New points are found as f -images of suitable points from the part we already computed. We stress that the idea of growing the manifold for a prescribed distance in each step has an immediate parallel in higher dimensions; see Section 4.

There are two methods that do not use iteration of a fundamental domain, which can also be used to compute unstable manifolds of higher dimension. First, there is the computation of *straddle trajectories* on codimension-1 unstable manifolds [21]. This method is computationally expensive and runs into difficulties if the manifold is complicated. Second, there is the method of finding an *outer approximation* of $W^u(x_0)$ by rectangular cells [5, 6, 23]. This method is very useful to get a global picture of a compact invariant manifold of moderate dimension, and it can also be used to compute invariant measures [7]. However, it does not give the parametrization of the manifold by arclength and may have difficulties showing small details.

3. THE 1D ALGORITHM

Starting with a linear approximation of the local unstable manifold our algorithm grows the manifold up to a prespecified arclength l with a speed depending on the curvature. The 1D algorithm has recently been implemented for use in the DsTool [2] environment; see [19] for details.

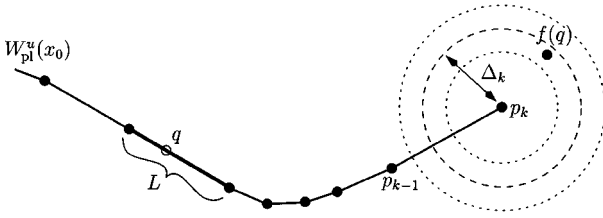


FIG. 1. The next point $p_{k+1} = f(q)$ is chosen at (approximately) distance Δ_k from p_k .

Recall that $f: \mathbb{R}^2 \rightarrow \mathbb{R}^2$ is an orientation preserving diffeomorphism with a saddle point $f(x_0) = x_0$. The algorithm produces a list $P = \{p_0, p_1, \dots, p_N\}$ of mesh points on the unstable manifold $W^u(x_0)$ starting with the fixed point $p_0 = x_0$ and the point p_1 at a small distance δ from x_0 in the unstable eigenspace $E^u(x_0)$. The total number N of points is variable and depends on the accuracy of the computation and the requested arclength l . During the computation we need the *continuous object* $W_{pl}^u(x_0)$, which is the piecewise linear approximation of the computed part of $W^u(x_0)$ formed by the line segments between consecutive mesh points. Initially, $W_{pl}^u(x_0)$ is the interval $[p_0, p_1]$; that is, it is the linear approximation of $W_{loc}^u(x_0)$. As we grow the manifold, points are added to P in steps, and $W_{pl}^u(x_0)$ changes accordingly.

We now describe a single step and suppose that $P = \{p_0, p_1, \dots, p_k\}$ is already known. The next point p_{k+1} should have the property that the line segment $[p_k, p_{k+1}]$ accurately approximates $W^u(x_0)$. Hence, the curvature of $W^u(x_0)$ determines the allowed distance between p_k and p_{k+1} . The idea is to use a guess Δ_k for this distance and find a candidate for p_{k+1} . Then we use the strategy of [13] to determine whether the guessed distance Δ_k was acceptable, meaning that the interpolation error is within the desired accuracy. How this is done is explained in the next section.

Using the estimate Δ_k , we want to find p_{k+1} in a small annulus around the circle centered at p_k with radius Δ_k ; see Fig. 1. To this end, we search in $W_{pl}^u(x_0)$ for the line segment L that is mapped by f to a curve which intersects the circle with center p_k and radius Δ_k . We start this search with the line segment in $W_{pl}^u(x_0)$ that contains the preimage of p_k and move linearly through $W_{pl}^u(x_0)$. Once L is found, we use bisection to find a point $q \in L$ such that

$$(1 - \varepsilon)\Delta_k < \|f(q) - p_k\| < (1 + \varepsilon)\Delta_k.$$

The uncertainty factor ε is used to reduce the number of bisection steps. (In Section 3.3 this value is fixed to $\varepsilon = 0.2$.)

The point $p_{k+1} := f(q)$ is a candidate for the next point in P . We will accept $f(q)$ provided our guess for the distance Δ_k was not too large, according to the criterion in the next section. If Δ_k is acceptable then $p_{k+1} = f(q)$ is added to P , $[p_k, p_{k+1}]$ is added to $W_{pl}^u(x_0)$, and the step is complete. However, if Δ_k was too large then we reject $f(q)$, halve the estimate Δ_k , and repeat the process.

It may not be possible to find a point p_{k+1} at (approximately) distance Δ_k from p_k . This occurs when $W^u(x_0)$ is of finite arclength, because $W^u(x_0)$ is attracted to a point attractor. In this situation we also halve Δ_k and try again. We detect convergence of the manifold to an attractor if Δ_k drops below a predefined bound.

3.1. Monitoring the Distance Δ_k

For completeness we describe our method for monitoring the distance Δ_k , which is (a slight variation of) Hobson's strategy in [13]. We say that $W_{\text{pl}}^u(x_0)$ accurately approximates $W^u(x_0)$ if the maximal error ε_{pl} between $W_{\text{pl}}^u(x_0)$ and the corresponding first finite piece of $W^u(x_0)$ is small. The error ε_{pl} depends on the distances Δ_k between consecutive mesh points. In order to keep the interpolation error on the linear line segment of $W_{\text{pl}}^u(x_0)$ small, the allowed distance between mesh points must be adapted to the local curvature of $W^u(x_0)$. If $W^u(x_0)$ is locally almost a straight line, only a few mesh points are required, whereas many points are needed where $W^u(x_0)$ has sharp folds.

Assume that we have found a candidate $p_{k+1} = f(q)$ in a small annulus around the circle with center p_k and radius Δ_k . We need to check whether Δ_k is an allowed distance. To determine this, we approximate the angle α between the lines through p_{k-1} , p_k and p_k , p_{k+1} , by

$$\alpha_k = \frac{\|\bar{p} - p_{k-1}\|}{\|p_k - p_{k-1}\|}, \quad (1)$$

where $\bar{p} = p_k + (p_k - p_{k+1})/\|p_k - p_{k+1}\|$; compare [13]. Then, we check the conditions

$$\begin{aligned} \alpha_{\min} < \alpha_k < \alpha_{\max} \\ (\Delta\alpha)_{\min} < \Delta_k \alpha_k < (\Delta\alpha)_{\max}, \end{aligned} \quad (2)$$

where the bounds are four prespecified control parameters. The first condition states that α_k should be small, which will avoid that the algorithm cuts off edges in sharp folds. The second condition controls the local interpolation error.

If both $\alpha_k < \alpha_{\max}$ and $\Delta_k \alpha_k < (\Delta\alpha)_{\max}$ then Δ_k is acceptable. We use $\Delta_{k+1} = \Delta_k$ unless Δ_k is rather small, that is, when both $\alpha_k < \alpha_{\min}$ and $\Delta_k \alpha_k < (\Delta\alpha)_{\min}$. In this case, we set $\Delta_{k+1} = 2\Delta_k$. On the other hand, if $\alpha_k \geq \alpha_{\max}$ or $\Delta_k \alpha_k \geq (\Delta\alpha)_{\max}$ then Δ_k is too large, and we set $\Delta_k = \frac{1}{2}\Delta_k$ and try again. Similar to [13], we use a lower bound Δ_{\min} on Δ_k .

3.2. Discussion of the Accuracy

The accuracy of a computation depends on the distribution of mesh points and the initial distance along $E^u(x_0)$. The initial error between the first line segment in the linear unstable eigenspace $E^u(x_0)$ and the local unstable manifold $W_{\text{loc}}^u(x_0)$ is controlled by the initial distance δ from the fixed point x_0 . Since $W^u(x_0)$ is a collection of f -images of $W_{\text{loc}}^u(x_0)$, and since forward iterates converge in stable directions near x_0 , this initial error will be damped in a neighborhood of the fixed point. However, outside a local neighborhood, the initial error grows with the number of iterates of the line segment that are needed to cover the computed part. We get an additional error ε_I from the interpolation between the mesh points, because we grow the manifold by taking images of interpolated points. In [13] it is shown that the interpolation error ε_I is controlled by keeping the product $\Delta_k \alpha_k$ small. The total error ε_{pl} depends on the initial error and the interpolation error. Because we compute only a finite piece of $W^u(x_0)$, ε_{pl} is bounded, and it goes to zero for $\delta \rightarrow 0$ and $\varepsilon_I \rightarrow 0$; we refer to the proofs in [13] and [20].

A special issue is the problem of cutting off folds. It may seem that the 1D algorithm cuts off sharp folds, because the point p_k might have been chosen on the returning branch;

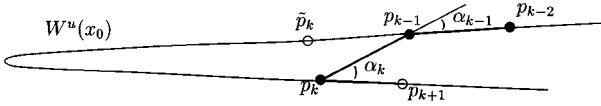


FIG. 2. A situation where part of the manifold might be missed.

see Fig. 2. The point p_k would have been accepted, because $\Delta_{k-1} = \|p_k - p_{k-1}\|$ and α_{k-1} satisfy (2). However, an early jump to the returning branch can only occur when the fold is very sharp and the preimage between p_{k-1} and p_k is contained in a single interval. By properly choosing α_{\max} we can ensure that this is not the case, since a sharp fold generally has a milder fold as preimage. In other words, instead of p_k , the other candidate \tilde{p}_k is found, and the fold is not missed; see Fig. 2 and the examples in the next section.

The above arguments show that a finite piece of the unstable manifold can be computed with any desired precision if the accuracy parameters are chosen small enough. The main problem of any global manifold computation is that, in general, a priori bounds on the accuracy parameters are not available. A good way to check the accuracy in practice is to repeat the computation with increased accuracy and to compare the results.

3.3. Examples of 1D Manifolds

In this section we demonstrate the 1D algorithm with two planar maps, the shear map and the IBV map, that we feel are ideal for testing any algorithm for the computation of global unstable manifolds. The shear map, a constructed example, has homoclinic tangencies to a segment of the coordinate axes. The IBV map is a generalization of a map in [1, 17] describing chaotic fluid mixing in a stirred tank, and it is characterized by strong recursive spiraling. See also [18, 19] for (un)stable manifolds of the Poincaré map of the forced damped pendulum and of the forced Van der Pol oscillator, respectively.

3.3.1. The shear map. In this section we introduce the *shear map*, a one-parameter family of diffeomorphisms on \mathbb{R}^2 , with the following special properties. The origin is always a saddle point such that the stable and unstable manifolds contain parts of the coordinate axes. Furthermore, the family has a first homoclinic tangency for a particular parameter value, called c^* . Since one of the manifolds involved in the tangency is equal to a coordinate axis near the origin, we can approximate c^* by checking whether the other manifold returns tangent to this axis.

An abstract presentation of the shear map can be found in [25]. Here, we give a concrete definition. We start with the linear map

$$\phi \begin{pmatrix} x \\ y \end{pmatrix} = \begin{pmatrix} \lambda^u x \\ \lambda^s y \end{pmatrix},$$

where $0 < \lambda^s \leq (\lambda^u)^{-1} < 1$ are fixed. Clearly, the origin $\mathbf{0}$ is a saddle point of ϕ and its stable and unstable manifolds are the coordinate axes. Consider now the one-parameter family of maps

$$\psi_c \begin{pmatrix} x \\ y \end{pmatrix} = \begin{pmatrix} x - cf(x+y) \\ y + cf(x+y) \end{pmatrix},$$

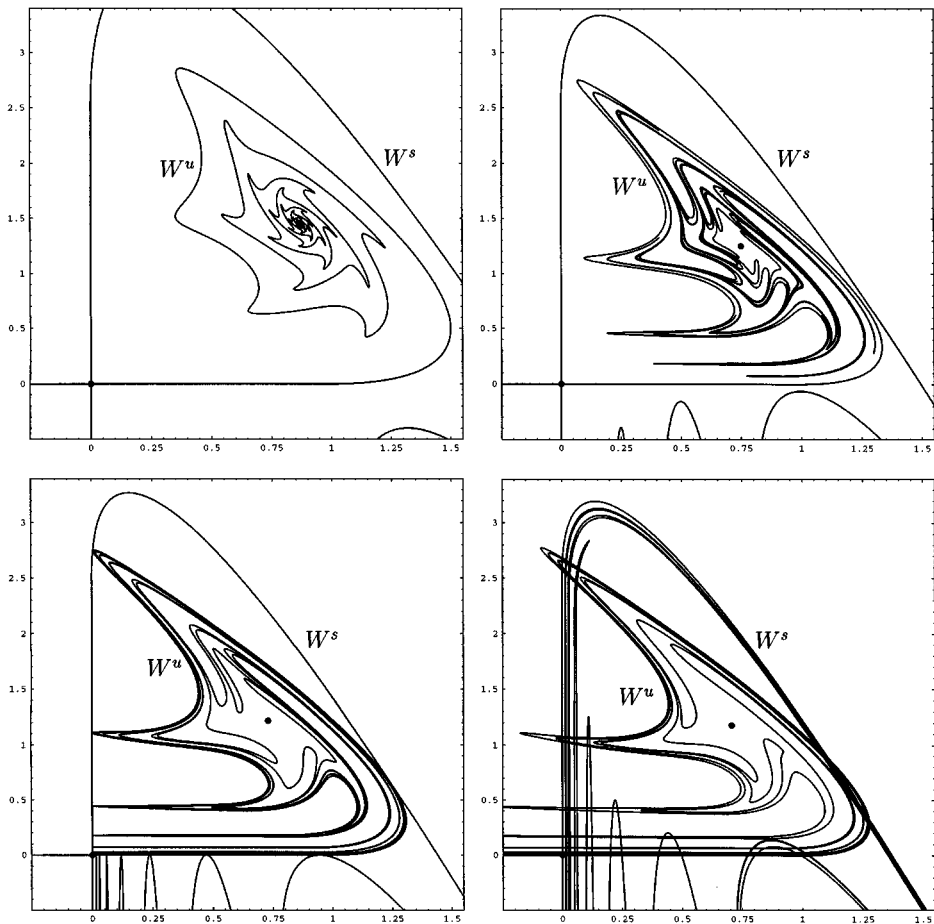


FIG. 3. Stable and unstable manifolds of the origin of the shear map before (top), approximately at (bottom left), and after (bottom right) the first tangency. ($c = 0.5$, $c = 0.75$, $c = 0.811580$, and $c = 0.9$, respectively; branch of $W^u(\mathbf{0})$ computed up to arclength 100, branch of $W^s(\mathbf{0})$ computed up to arclength 5000.)

where

$$f(z) = \begin{cases} 0 & \text{for } z \leq 1 \\ (z-1)^2 & \text{for } z > 1. \end{cases}$$

The map ψ_c shears the plane, because it is a drift of magnitude $\sqrt{2}cf(x+y)$ along the diagonal lines $\{(x, y) \mid x+y = \text{const} > 1\}$. The shear map is now defined as the composition

$$\Psi_c = \psi_c \circ \phi. \quad (3)$$

By construction of Ψ_c the origin $\mathbf{0}$ is a saddle point for any c , with eigenvalues λ^u and λ^s . Furthermore, the interval $\{x \in (-\infty, 1], y = 0\}$ is contained in $W^u(\mathbf{0})$, and $\{y \in (-\infty, (\lambda^s)^{-1}], x = 0\}$ is contained in $W^s(\mathbf{0})$. There is a first homoclinic tangency for a particular $c^* \in [0, \lambda^u]$; see [18, 25].

Throughout our computations we have chosen $\lambda^s = 0.4$ and $\lambda^u = 2.0$. Figure 3 shows the stable and unstable manifolds before the tangency for $c = 0.5$ and $c = 0.75$ (top), approximately at the tangency for $c = 0.811580$ (lower left), and after the tangency for $c = 0.9$

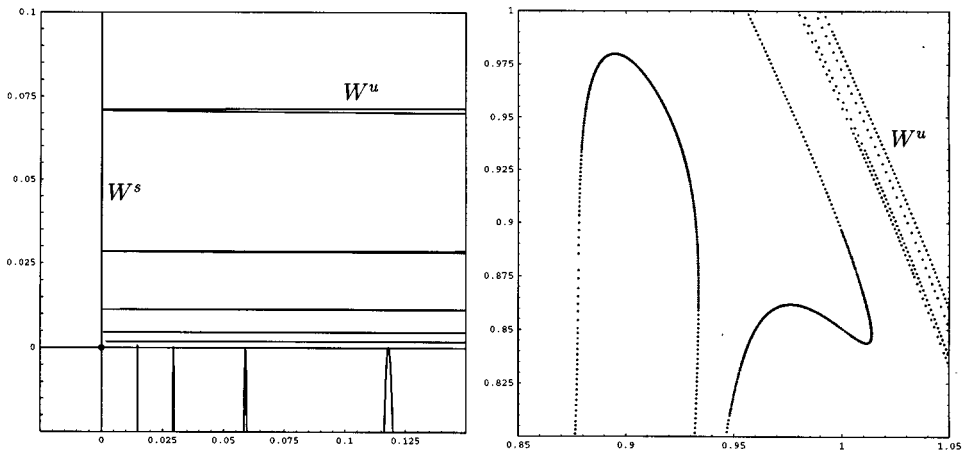


FIG. 4. Enlargement near the fixed point (left) of Fig. 3, and of a part of $W^u(\mathbf{0})$ (right) showing the distribution of the computed points. ($c = 0.811580$; branch of $W^u(\mathbf{0})$ computed up to arclength 100.)

(lower right). The accuracy was $\alpha_{\min} = 0.2$, $\alpha_{\max} = 0.3$, $(\Delta\alpha)_{\min} = 10^{-6}$, $(\Delta\alpha)_{\max} = 10^{-5}$, and $\Delta_{\min} = 10^{-4}$. (Recall that $\varepsilon = 0.2$ in all computations.) We chose $\delta = 10^{-3} < 1$, such that $W_{\text{loc}}^u(\mathbf{0})$ and $W_{\text{loc}}^s(\mathbf{0})$ are exact. The respective unstable branches have been computed up to arclength 100, and the stable branches up to arclength 5000. (The stable manifolds make very long excursions into the lower half plane.) The arclength of the unstable manifold is finite for $c < c^*$, but goes to infinity as $c \rightarrow c^*$. Indeed, for $c = 0.5$ the computation of $W^u(\mathbf{0})$ stops at arclength $l = 19.53$ when $\Delta_k < 10^{-12}$. For $c = 0.8$ the arclength of $W^u(\mathbf{0})$ is already larger than 100.

Figure 4 (left) shows an enlargement near the origin at the approximate moment of first tangency ($c = 0.811580$). A numerically found tangency is never exactly a tangency. Due to the Λ -Lemma [24], this will become clearly visible for a suitable iterate, that is, when longer pieces of the manifolds are computed. Making sure that $W^u(\mathbf{0})$ and $W^s(\mathbf{0})$ have tangencies along the entire computed arclength allows one to find the value of c^* with any precision. (We found $c^* \approx 0.811580$, which is precise up to five digits.) Clearly, this also requires one to compute $W^u(\mathbf{0})$ and $W^s(\mathbf{0})$ with sufficient accuracy. It is an interesting observation that looking at long pieces of $W^u(\mathbf{0})$ and $W^s(\mathbf{0})$ also allows one to check the accuracy of the computed manifolds themselves. If one looks closely one notices that the last loop of $W^s(\mathbf{0})$ just intersects $W^u(\mathbf{0})$. On the other hand, the last loop of $W^u(\mathbf{0})$ just misses $W^s(\mathbf{0})$. This is theoretically impossible, and it shows that $W^u(\mathbf{0})$ and $W^s(\mathbf{0})$ have not been computed accurately over the entire prescribed arclength. The solution is to choose higher accuracy, which would allow us to make sure that all computed tangencies lie on the coordinate axes.

To give an idea of how the mesh depends on the curvature, Fig. 4 (right) shows an enlargement of the unstable manifold for $c = 0.811580$. The points are not connected to show their distribution, which is clearly adapted to the curvature. Note that the distance between neighboring points varies slightly because of the uncertainty factor $\varepsilon = 0.2$.

3.3.2. The IBV map. We consider a planar map of the complex plane, which we call the *IBV map*, modeling two independent blinking vortices in an infinitely large container with a thin layer of fluid (with possible injection or drainage of fluid at the vortices). This

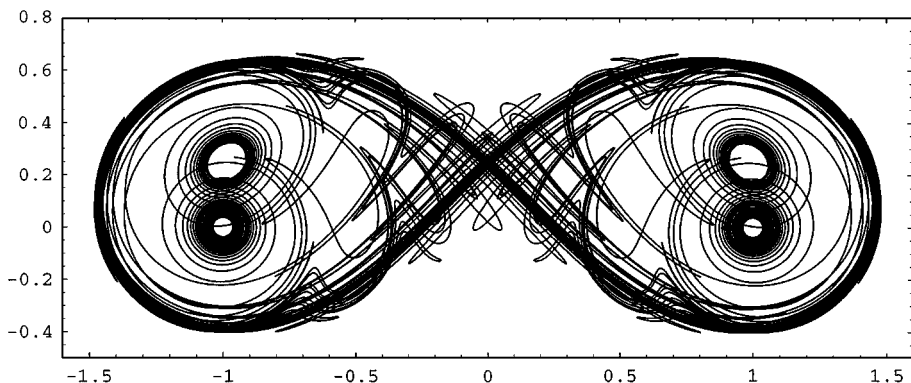


FIG. 5. Homoclinic tangle of the fixed point $z_0 \approx 0.241988i$ of the conservative IBV map with the same direction of rotation. ($b_1 = b_2 = 1$, $\mu_1 = \mu_2 = 0.08$; all branches computed up to arclength 100.)

map is a generalization of Aref's blinking vortex map in [1, 17], which was introduced as an idealized model of chaotic mixing. Recently, the dynamics near one vortex was studied in [30]. A vortex at the origin is described by the map

$$R_{\mu,b}(z) = bz \exp\left(2\pi i \frac{\mu}{|z|^2}\right), \quad R_{\mu,b}(0) = 0,$$

where μ specifies the amount of rotation at the unit circle, and $b \in (0, \infty)$ models injection or drainage of fluid. The IBV map is now obtained by considering two independent vortices v_1 at $+1$ and v_2 at -1 . We first shift the point v_1 to the origin, apply a vortex map, shift the point v_2 to the origin, apply another vortex map, and finally shift the origin back to v_2 . In other words, the IBV map is the composition

$$\Phi_{\mu_1, b_1, \mu_2, b_2} = T_{-1} \circ R_{\mu_2, b_2} \circ T_2 \circ R_{\mu_1, b_1} \circ T_{-1}, \quad (4)$$

where $T_c(z) = z + c$ is the translation by c . The IBV map (4) is continuous, has a continuous inverse on \mathbb{C} , and is differentiable on $\mathbb{C} \setminus \{+1, 1 - 2 \exp(-\pi i \mu_1 b_1^2 / 2) / b_1\}$. The map depends on four real parameters and has rich dynamics. The conservative case ($b_1 = b_2 = 1$) with the same direction of rotation ($\mu_1 = \mu_2$) reduces to Aref's blinking vortex map [1, 17]. The map studied in [30] can be interpreted as the limit $\mu_1, \mu_2 \rightarrow 0$ in a rescaled neighborhood of one of the vortices. Note that the map Φ also allows one to consider the case of counterrotating vortices ($\mu_1 = -\mu_2$), which does not seem to have been studied.

First we consider an example of the conservative case of corotating vortices studied in [1, 17]. We set $b_1 = b_2 = 1$ and $\mu_1 = \mu_2 = 0.08$, for which Φ has the saddle point $z_0 \approx 0.241988i$. Its stable and unstable manifolds, both computed up to arclength 100, form the homoclinic tangle shown in Fig. 5; compare Fig. 12 in [17]. Note that, by virtue of the map, the unstable manifold is the image of the stable manifold under the symmetry transformation $z \mapsto -\bar{z}$. The size of the lobes of the homoclinic intersections determines how much fluid is transported between the two sides of the figure-eight-shaped region. The accuracy of the computation is $\delta = 10^{-3}$, $\alpha_{\min} = 0.2$, $\alpha_{\max} = 0.3$, $(\Delta\alpha)_{\min} = 10^{-5}$, $(\Delta\alpha)_{\max} = 10^{-4}$, and $\Delta_{\min} = 5 \times 10^{-3}$.

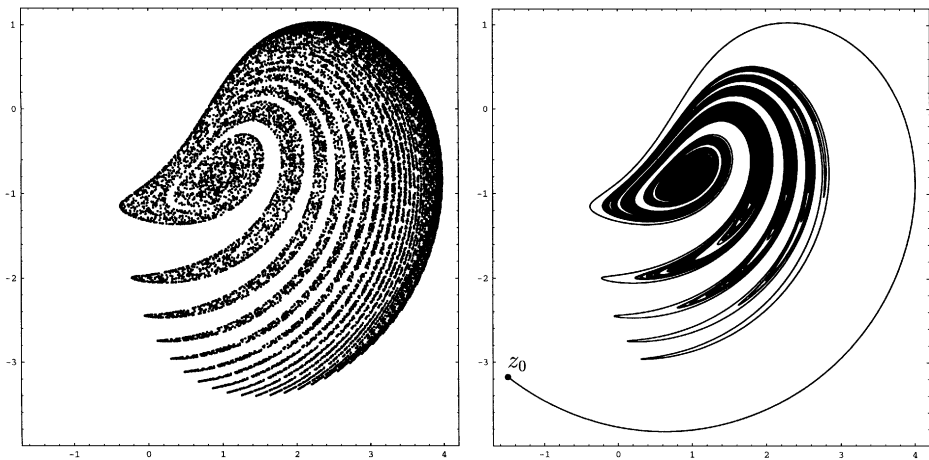


FIG. 6. The strange attractor (left) of the dissipative IBV map with opposite directions of rotation attracts one branch of the unstable manifold of the fixed point $z_0 \approx -1.49477 - 3.17655i$ (right). ($b_1 = 1.05, b_2 = 0.9, \mu_2 = -\mu_1 = 0.25$; branch of $W^u(x_0)$ computed up to arclength 10,000.)

As a second example we choose a case of counterrotating vortices with injection and drainage, namely, $b_1 = 1.05, b_2 = 0.9$, and $\mu_2 = -\mu_1 = 0.25$. Then Φ has the strange attractor shown in Fig. 6 (left). This has been obtained with DsTool [2] by recording 20,000 iterates after discarding a sufficiently long transient. We computed one branch of the unstable manifold of the saddle point $z_0 \approx -1.49477 - 3.17655i$ up to an arclength of 10,000. To keep the amount of data manageable we used the relatively low accuracy of $\delta = 10^{-3}, \alpha_{\min} = 0.2, \alpha_{\max} = 0.3, (\Delta\alpha)_{\min} = 10^{-3}, (\Delta\alpha)_{\max} = 10^{-2}$, and $\Delta_{\min} = 5 \times 10^{-3}$, which resulted in a total of 289,594 mesh points. The manifold is shown in Fig. 6 (right). While it is attracted to the strange attractor, it spirals repeatedly and recursively into the center of the picture, before making spiraling excursions into the “fingers.” Hence, the unstable manifold gives better insight into the dynamics on the attractor. A very long piece of the manifold is needed in order to see excursions to the fourth finger. One can get an idea of the accuracy of the computation by noticing that the tips of all four fingers indeed coincide with the respective tips of the attractor; compare the two panels of Fig. 6.

4. THE Q2D ALGORITHM

Quasiperiodically forced systems appear naturally in systems with two different periodic forcings of incommensurable frequencies. By taking the Poincaré map, or stroboscopic map, corresponding to one of these frequencies, one obtains a discrete dynamical system of the form

$$f \begin{pmatrix} \vartheta \\ x \end{pmatrix} = \begin{pmatrix} \vartheta + \omega \\ f_1(\vartheta, x) \end{pmatrix}, \tag{5}$$

where $\vartheta \in [0, 1)$ and $x \in \mathbb{R}^n$. Here, $\omega \in \mathbb{R} \setminus \mathbb{Q}$ is the irrational ratio between the two frequencies, and f_1 is periodic in ϑ with period 1. Quasiperiodically forced systems have drawn special attention because they exhibit transitions to chaos via so-called strange nonchaotic attractors that seem to be unique to this class of dynamical systems; see [8, 29]. We consider the case $n = 2$ such that (5) has a three-dimensional state space.

Because of the quasiperiodic forcing, the smallest invariant sets of (5) are closed invariant curves that can be parametrized by ϑ . When restricted to such an invariant circle, the system is just a rigid rotation with irrational rotation number ω . Let us assume that (5) has an invariant circle $H = \{(\vartheta, h(\vartheta) \mid \vartheta \in [0, 1)\}$ of saddle type with a two-dimensional unstable manifold, denoted by $W^u(H)$.

In order to compute $W^u(H)$ we consider its intersection curves with planes of the form $\mathcal{F}_\theta = \{(\vartheta, x) \mid \vartheta = \theta\}$. These planes foliate the phase space $[0, 1) \times \mathbb{R}^2$. Because of the special structure of (5), the linear foliation $\{\mathcal{F}_\theta\}_{\theta \in [0, 1)}$ is f -invariant, H intersects each leaf \mathcal{F}_θ in a unique point, and $W^u(H)$ intersects \mathcal{F}_θ in a unique curve for all $\theta \in [0, 1)$.

The idea is now to grow the intersection curves $W^u(H) \cap \mathcal{F}_\theta$ simultaneously in a prescribed number of leaves. We take a finite number of leaves \mathcal{F}_θ by choosing a mesh M on $[0, 1)$, equally spaced for simplicity. As starting data we need to know $H \cap \{\mathcal{F}_\theta\}_{\theta \in M}$, together with the linear unstable directions given as vectors $\{v^u(\theta)\}_{\theta \in M}$. Both can be obtained with the method in [3, 4, 22]. The manifold is represented in the form of the list $\{P_\theta\}_{\theta \in M}$ of sequences P_θ of points on $W^u(H) \cap \mathcal{F}_\theta$.

Again, we grow $W^u(H)$ in steps, where in each step one point is added to *each* P_θ for all $\theta \in M$. To this end, for each $\theta \in M$ we need to find a point q that gets mapped into \mathcal{F}_θ at distance Δ_k from the last point in P_θ . Because of the structure of (5), $q \in \mathcal{F}_{\theta-\omega}$, so that we can find q in the unique curve $W^u(H) \cap \mathcal{F}_{\theta-\omega}$ by bisection just as for the 1D algorithm. Note that $\theta - \omega$ will not be in the mesh M . Therefore, we approximate $W^u(H) \cap \mathcal{F}_{\theta-\omega}$ as a list of points $P_{\theta-\omega}$ by linear interpolation with its direct neighbors, say P_{θ_1} and P_{θ_2} , by

$$P_{\theta-\omega}(i) = P_{\theta_1}(i) + \frac{\theta_1 - (\theta - \omega)}{\theta_1 - \theta_2} (P_{\theta_2}(i) - P_{\theta_1}(i)).$$

In $P_{\theta-\omega}$ we now search for q exactly as we did in the 1D algorithm.

The distribution of points in P_θ is adapted to the curvature of $W^u(H) \cap \mathcal{F}_\theta$, such that $W_{\text{pl}}^u(\theta)$ is a good approximation of $W^u(H) \cap \mathcal{F}_\theta$; see Section 3.1. To ensure the quality of the two-dimensional mesh $\{P_\theta\}_{\theta \in M}$ we would like to have uniform growth in each leaf. This is also important for keeping new points in neighboring leaves quite close together, which ensures the quality of the interpolated sequences $P_{\theta-\omega}$. Ideally, at step k the distance Δ_k of the last point to the newly added point in P_θ is the same for all $\theta \in M$. (Clearly, Δ_k must be such that the accuracy of $W_{\text{pl}}^u(h(\theta))$ is acceptable for all $\theta \in M$.) However, a fold in the manifold, requiring more mesh points or slower growth, is typically reached at different arclength distances from H in each leaf. Slowing to the speed in the “slowest” leaf creates unnecessarily many mesh points in the other leaves.

To avoid producing too many points we proceed as follows. Note that in terms of the mesh quality the fundamental length scale is the distance between neighboring leaves of $\{\mathcal{F}_\theta\}_{\theta \in M}$ (which is $1/|M|$ for an equally spaced mesh). At step k , we determine the acceptable distance Δ_θ in P_θ for each $\theta \in M$. If $\Delta_k = \min_{\theta \in M} \Delta_\theta$ is still relatively large (compared to the distance between neighboring leaves) then we grow the manifold for the same distance Δ_k in each leaf. Otherwise, we allow variable steps, but such that $\max_{\theta \in M} \Delta_\theta$ is small enough. This works particularly well if the manifold folds over the entire θ -range, but at different arclength distances in different leaves; see Fig. 7 (left). We remark that permitting different Δ_θ -steps in different leaves also allows the two-dimensional manifold to converge to an attractor.

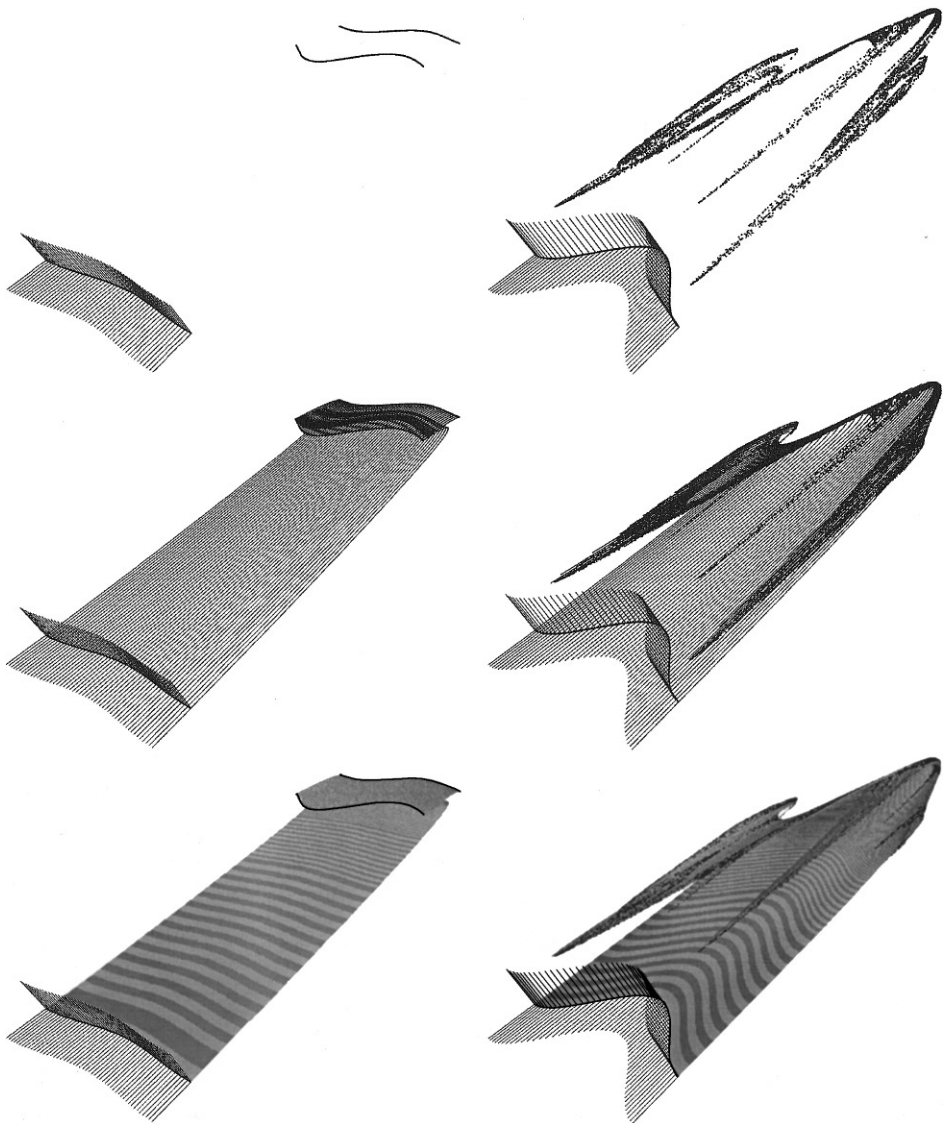


FIG. 7. The quasiperiodically forced Hénon map for $A=0.1$, $b=0.68$, and $c=0.1$ (left), and $A=0.7$, $b=0.77$, and $c=0.1$ (right). Initial data at 50 mesh points with the attractors (top), the curves $W^u(H) \cap \mathcal{F}_\theta$ for 50 θ -values (middle), and the manifold as a surface (bottom).

4.1. Examples of Q2D Manifolds

We illustrate the Q2D algorithm with the quasiperiodically forced Hénon map

$$f \begin{pmatrix} \vartheta \\ u \\ v \end{pmatrix} = \begin{pmatrix} \vartheta + \omega \\ 1 + v - bu^2 + A \cos(2\pi\vartheta) \\ cu \end{pmatrix}, \tag{6}$$

where we fix $\omega = \frac{1}{2}(\sqrt{5} - 1)$. This map is studied in [29] and is used in [20] as an example for the general algorithm.

First we choose $A = 0.1$, $b = 0.68$, and $c = 0.1$. Then (6) has an invariant circle H of saddle type with a two-dimensional unstable manifold that is attracted to a pair of circles of period two, folding infinitely often in the process. We chose 100 equally spaced mesh points on H and computed the starting data with the method in [3, 4, 22]. Figure 7 (top left) shows the circle H with the linear stable and unstable directions, and the period-two attracting circles. For the accuracy parameters we used $\delta = 0.01$, $\alpha_{\min} = 0.2$, $\alpha_{\max} = 0.3$, $(\Delta\alpha)_{\min} = 10^{-5}$, $(\Delta\alpha)_{\max} = 10^{-4}$, and $\Delta_{\min} = 10^{-4}$. In order to keep the mesh squared, we brought back the uncertainty factor to $\varepsilon = 0.01$. Figure 7 (middle left) shows the intersection curves of every second leaf, computed up to arclength 10. The manifold itself is shown in Fig. 7 (bottom left), where the gray bands show the steps taken in the Q2D algorithm. We previously computed the same manifold with the general algorithm, but could only get to the second fold; compare Fig. 11 in [20]. With the Q2D algorithm we can compute many more folds. This is clear from Fig. 8 (left), which shows the intersection of the manifold with $\mathcal{F}_{0.1}$ and two enlargements thereof.

As a second example we choose $A = 0.7$, $b = 0.77$, and $c = 0.1$. Then the invariant circle H still exists, but there is now a strange (and chaotic) attractor; compare Fig. 1(c) in [29]. Figure 7 (top right) shows the starting data and the attractor. We computed the unstable manifold $W^u(H)$, again with 100 leaves and the same accuracy as above. Figure 7 (middle right) shows the intersection curves of every second leaf, again up to arclength 10, and Fig. 7 (bottom right) shows the manifold itself. As our computation shows, the unstable manifold converges to the strange attractor. The intersection of the unstable manifold with $\mathcal{F}_{0.1}$ and two enlargements are shown in Fig. 8 (right). An approximation of the intersection of the strange attractor with $\mathcal{F}_{0.1}$ was found by iterating 1000 points. The attractor intersects this leaf in what appears to be a curve, approximated by the bold dots in Fig. 8 (right). Animations showing how manifolds are grown by the Q2D algorithm can be found at <http://www.nat.vu.nl/vakgroepen/theorie/english/publications/eprints/vuth98-21/vuth98-21.html>.

4.2. Remarks on the General Case

The idea of growing the intersection curves of a two-dimensional unstable manifold with a set of planes is also behind the general 2D algorithm in [20]. The general algorithm can be used for the special class of quasiperiodically forced systems, but the specialized Q2D algorithm is superior. It is powerful and fast, because it is a true generalization of the 1D algorithm.

The special purpose Q2D algorithm performs better for the following reasons. In general, any foliation of phase space by planes is *not* invariant under the map. This means that we do not know a priori in which leaf we should look for the point q . Consequently, we have to do a more time-consuming 2D search. A major disadvantage of a 2D search is that one lacks a clear direction in which to look for q starting at the preimage of the last point. If the manifold folds sharply, then it is virtually impossible for the general algorithm to avoid that the manifold grows “backward.” This is why the general algorithm stops at the second fold of the manifold in Fig. 7 (left); compare Fig. 11 in [20].

Finally, for a quasiperiodically forced system, the intersection of $W^u(H)$ with a leaf \mathcal{F}_θ is a unique curve. For a general map, this is usually not true for any chosen linear foliation. Locally near H it can always be achieved, but as one grows $W^u(H)$, the manifold may become tangent to a leaf. At that point, a second intersection curve, not connected to the

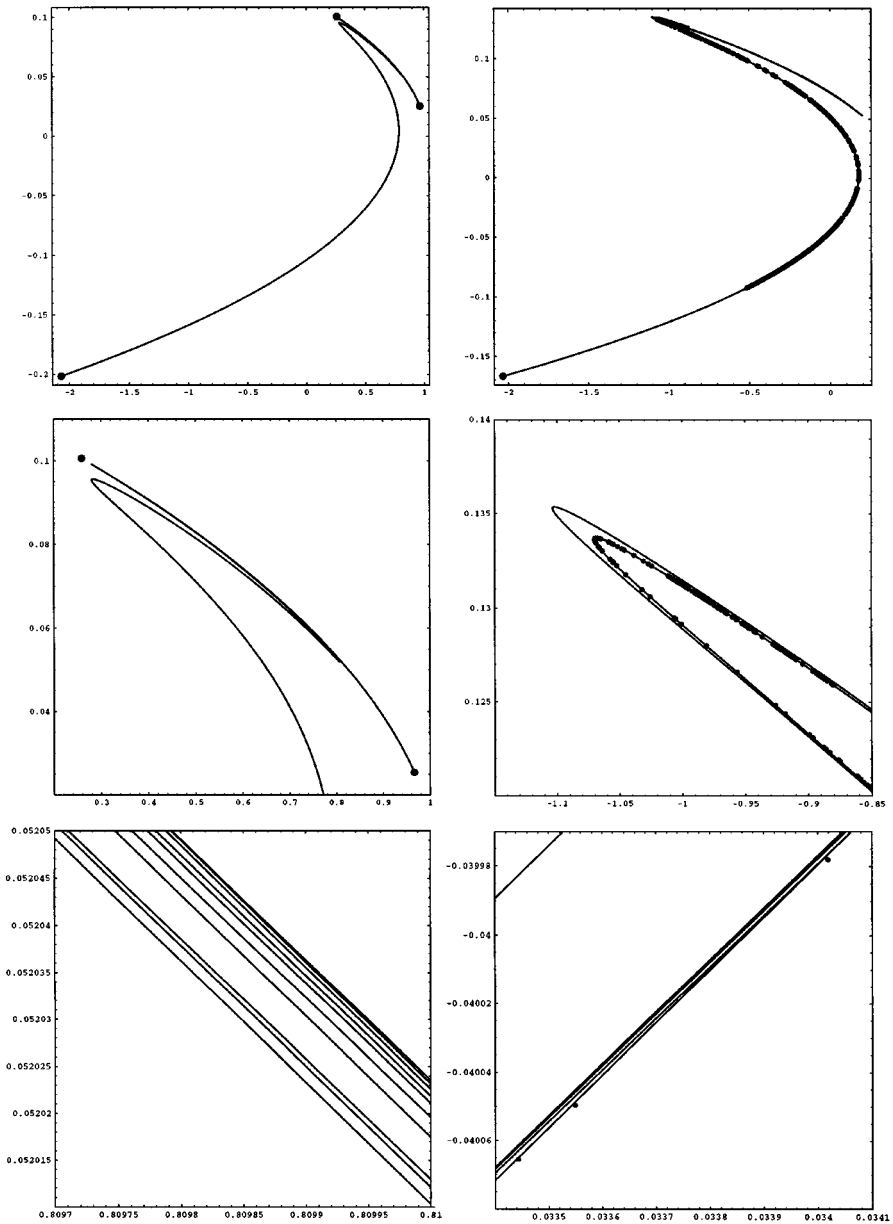


FIG. 8. Intersections of the manifolds and the attractors in Fig. 7 with the leaf $\mathcal{F}_{0,1}$ (top), and enlargements (middle and bottom).

first, appears in this leaf. In its current form, the general 2D algorithm in [20] misses this part of $W^u(H)$ and subsequently stops.

ACKNOWLEDGMENTS

B.K. is grateful for the hospitality and financial support of the Institute of Mathematics and its Applications and The Geometry Center, Minneapolis. H.O. thanks the Vrije Universiteit Amsterdam for its hospitality.

REFERENCES

1. H. Aref, Stirring by chaotic advection, *J. Fluid Mech.* **143**, 1 (1984).
2. A. Back, J. Guckenheimer, M. R. Myers, F. J. Wicklin, and P. A. Worfolk, DsTool: Computer assisted exploration of dynamical systems, *Notices Amer. Math. Soc.* **39**, 303 (1992).
3. H. W. Broer, H. M. Osinga, and G. Vegter, On the computation of normally hyperbolic invariant manifolds, in *Nonlinear Dynamical Systems and Chaos*, edited by H. W. Broer *et al.*, PNLDE (Birkhäuser Verlag, Basel, Switzerland, 1996), Vol. 19, p. 423.
4. H. W. Broer, H. M. Osinga, and G. Vegter, Algorithms for computing normally hyperbolic invariant manifolds, *Z. Angew. Math. Phys.* **48**, 480 (1997).
5. M. Dellnitz and A. Hohmann, The computation of unstable manifolds using subdivision and continuation, in *Nonlinear Dynamical Systems and Chaos*, edited by H. W. Broer *et al.*, PNLDE (Birkhäuser Verlag, Basel, Switzerland, 1996), Vol. 19, p. 449.
6. M. Dellnitz and A. Hohmann, A subdivision algorithm for the computation of unstable manifolds and global attractors, *Num. Math.* **75**, 293 (1997).
7. M. Dellnitz, A. Hohmann, O. Junge, and M. Rumpf, Exploring invariant sets and invariant measures, *Chaos* **7**, 221 (1997).
8. C. Grebogi, E. Ott, S. Pelikan, and J. A. Yorke, Strange attractors that are not chaotic, *Physica D* **13**, 261 (1984).
9. C. Grebogi, E. Ott, and J. A. Yorke, Crises, sudden changes in chaotic attractors, and transient chaos, *Physica D* **7**, 181 (1983).
10. J. Guckenheimer and P. Holmes, *Nonlinear Oscillations, Dynamical Systems, and Bifurcations of Vector Fields* (Springer-Verlag, New York/Berlin, 1983).
11. S. M. Hammel, C. K. R. T. Jones, and J. V. Moloney, Global dynamical behavior of the optical field in a ring cavity, *J. Opt. Soc. Am. B* **2**, 552 (1985).
12. M. Hénon, A two-dimensional mapping with a strange attractor, *Comm. Math. Phys.* **50**, 69 (1976).
13. D. Hobson, An efficient method for computing invariant manifolds of planar maps, *J. Comput. Phys.* **104**, 14 (1993).
14. A. J. Homburg, H. M. Osinga, and G. Vegter, On the computation of invariant manifolds of fixed points, *Z. Angew. Math. Phys.* **46**, 171 (1995).
15. A. J. Homburg, D. Sands, and R. de Vilder, *Computing Invariant Sets*, Technical Report 57/96, Schwerpunktprogramm Danse der DFG (1996).
16. K. Ikeda, H. Daido, and O. Akimoto, Optical turbulence: Chaotic behavior of transmitted light from a ring cavity, *Phys. Rev. Lett.* **45**, 709 (1980).
17. D. V. Khakhar, H. Rising, and J. M. Ottino, Analysis of chaotic mixing in two model systems, *J. Fluid Mech.* **172**, 419 (1986).
18. B. Krauskopf and H. M. Osinga, Growing unstable manifolds of planar maps, IMA preprint **1517** (1997); available at <http://www.ima.umn.edu/preprints/OCT97/1517.ps.gz>.
19. B. Krauskopf and H. M. Osinga, Investigating torus bifurcations in the forced Van der Pol oscillator, to appear in *Numerical Methods for Bifurcation Problems and Large-Scale Dynamical Systems*, edited by E. J. Doedel, B. Fiedler, I. G. Kevrekidis, W.-J. Beyn, J. Lorenz, L. Tuckerman, E. S. Titi, H. B. Keller, and D. G. Aronson, IMA Volumes in Mathematics and its Applications (Springer-Verlag, New York, 1999).
20. B. Krauskopf and H. M. Osinga, Globalizing two-dimensional unstable manifolds of maps, *Int. J. Bifurcation Chaos* **8**, 483 (1998).
21. H. E. Nusse and J. A. Yorke, A procedure for finding numerical trajectories on chaotic saddles, *Physica D* **36**, 137 (1989).
22. H. M. Osinga, *Computing Invariant Manifolds: Variations on the Graph Transform*, Ph.D. thesis, Groningen University (1996).
23. G. Osipenko, Localization of the chain recurrent set by symbolic dynamics methods, in *Proceedings of Dynamic Systems and Applications, Morehouse College, Atlanta, May 1993*, edited by G. S. Ladde and M. Sambandham (Dynamic Publishers, Atlanta, 1994), Vol. 1, p. 277.

24. J. Palis and W. de Melo, *Geometric Theory of Dynamical Systems* (Springer-Verlag, New York/Berlin, 1982).
25. J. Palis and F. Takens, *Hyperbolicity and Sensitive Chaotic Dynamics at Homoclinic Bifurcations* (Cambridge Univ. Press, Cambridge, UK, 1993).
26. T. S. Parker and L. O. Chua, *Practical Numerical Algorithms for Chaotic Systems* (Springer-Verlag, New York/Berlin, 1989).
27. M. Phillips, S. Levy, and T. Munzner, Geomview: An interactive geometry viewer, *Notices Amer. Math. Soc.* **40**, 985 (1993); this software and the accompanying manual are available at <http://www.geom.umn.edu/>.
28. C. Simó, On the analytical and numerical approximation of invariant manifolds, in *Les Méthodes Modernes de la Mécanique Céleste*, edited by D. Benest and C. Froeschlé (Goutelas, 1989), p. 285.
29. O. Sosnovtseva, U. Feudel, J. Kurths, and A. Pikovsky, Multiband strange nonchaotic attractors in quasiperiodically forced systems, *Phys. Lett. A* **218**, 255 (1996).
30. G. Stolovitzky, T. J. Kaper, and L. Sirovich, A simple model of chaotic advection and scattering, *Chaos* **5**, 671 (1995).
31. S. Wiggins, *Chaotic Transport in Dynamical Systems* (Springer-Verlag, New York/Berlin, 1992).
32. S. Wolfram, *Mathematica, A System for Doing Mathematics by Computer* (Addison-Wesley, Reading, MA, 1988).
33. Z. You, E. J. Kostelich, and J. A. Yorke, Calculating stable and unstable manifolds, *Int. J. Bifurcation Chaos* **1**, 605 (1991).